Chapter 4
A Silicon Model of Auditory Localization

The principles of organization of neural systems arose from the combination of the performance requirements for survival and the physics of neural elements. From this perspective, the extraction of time-domain information from auditory data is a challenging computation; the system must detect changes in the data that occur in tens of microseconds, using neurons that can fire only once per several milliseconds. Neural approaches to this problem succeed by closely coupling algorithms and implementation, unlike standard engineering practice, which aims to define algorithms that are easily abstracted from hardware implementation.

The echolocation system of the bat and the passive localization system of the barn owl are two neural systems that use extensive time-domain processing to create an accurate representation of auditory space. While the bat has developed specialized algorithms to implement an active sonar system, the barn owl and mammals use similar techniques to perform auditory localization. This chapter describes an integrated circuit that models, to a limited degree, the passive localization system of the barn owl.

The barn owl (*Tyto alba*) uses hearing to locate and catch small rodents in total darkness. The owl localizes the rustles of the prey to within 1 to 2 degrees in azimuth and elevation (Knudsen *et al.*, 1979). The owl cannot localize sounds when one ear is completely occluded; the auditory cues are differences in sound received by the two ears. The owl uses different binaural cues to determine azimuth and elevation. The elevational cue for the owl is binaural intensity difference. This cue is a result of a vertical asymmetry in the placement of the barn owl's ear openings, as well as a slight asymmetry in the left and right

halves of the barn owl's facial ruff, which acts as a sound-collecting device (Knudsen and Konishi, 1979). The azimuthal cue is binaural time difference. The binaural time differences are in the microsecond range, as expected from the short interaural distance of the owl, and vary as a function of azimuthal angle of the sound source (Moiseff and Konishi, 1981).

Unlike those in the visual system, the primary sensory neurons of the auditory system do not directly record the spatial location of a stimulus. Neuronal circuits must compute the position of sounds in space from acoustic cues in the stimulus. In the barn owl, the external nucleus of the inferior colliculus (ICx) contains the neural substrate of this computation, a spatial map of auditory space (Knudsen and Konishi, 1978). Neurons in the ICx respond maximally to stimuli located in a small area in space, corresponding to a specific combination of binaural intensity difference and binaural time difference (Figure 4.1). Recordings of the ICx neurons made while binaural intensity difference (Knudsen and Konishi, 1980) and binaural time difference (Moiseff and Konishi, 1981) are varied separately confirm the role of these acoustic cues.

There are several stages of neural processing between the primary sensory neurons at each cochlea and the computed map of space in the ICx. Each primary auditory fiber initially divides into two distinct pathways (Figure 4.2). One pathway processes intensity information, and thus encodes elevation cues, whereas the other pathway processes timing information, and thus encodes azimuthal cues. The two pathways recombine in the ICx to produce a complete map of space (Takahashi and Konishi, 1988b).

Recent anatomical and physiological studies provide a model of the structure and function of the time-coding pathway of the barn owl (Carr and Konishi, 1988; Takahashi and Konishi, 1988a; Fujita and Konishi, unpublished). This pathway has clear anatomical and physiological homologues in other avian

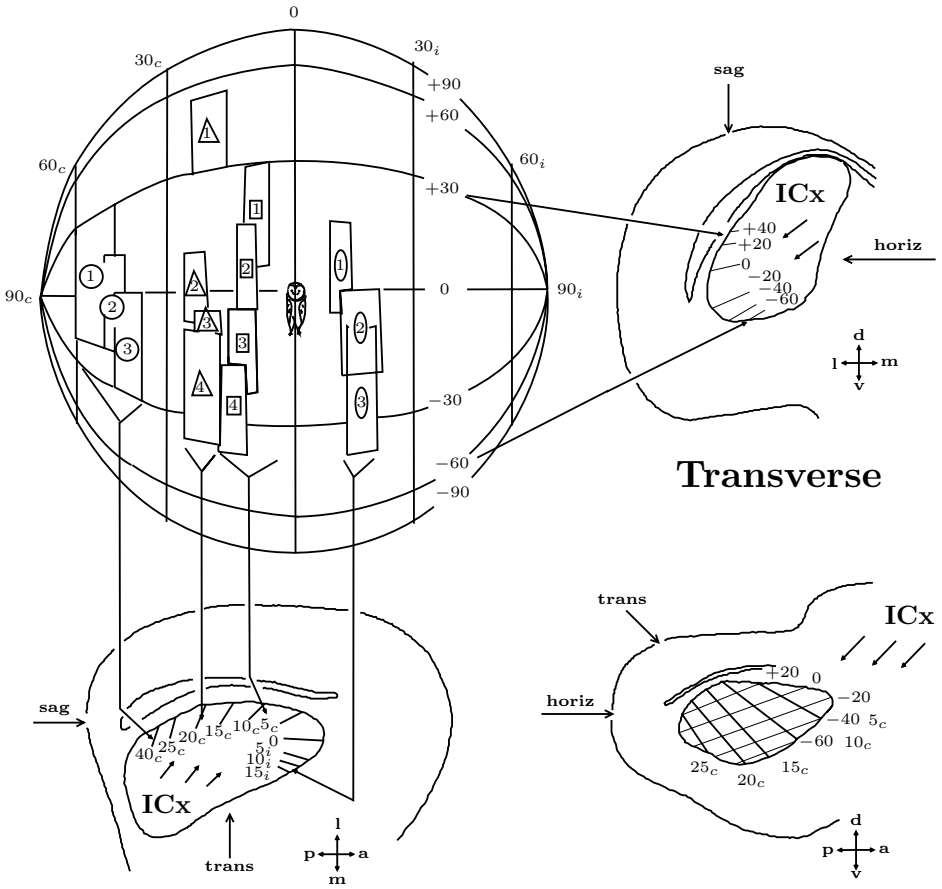
0
30_c
30_i
+90
+60
60_c
60_i
+30
90_c
0
90_i
−30
−60
−90
sag
ICx
+40
+20
0
−20
−40
−60
horiz
d
l
m
v
Transverse
trans
ICx
+20
0
horiz
−20
−40
5c
−60
10c
25c
20c
15c
sag
40c
25c
20c
15c
10c
5c
5i
0
10i
15i
ICx
trans
l
p
a
m
d
p
a
v
Horizontal
Sagittal

Figure 4.1. Neural map of auditory space in the barn owl. Auditory space is depicted as an imaginary globe surrounding the owl. Projected onto the globe are the receptive field best areas of 14 neurons. The best area, a zone of maximal response within a receptive field, remains unaffected by variations in sound intensity and quality. The numbers surrounding the same symbols (circles, rectangles, triangles, ellipses) represent neurons from the same electrode penetration; the numbers themselves denote the order in which the neurons were encountered. Below and to the right of the globe are illustrations of three histological sections through the inferior colliculus; arrows point to the external nucleus, the ICx. Iso-azimuth contours are shown as thick lines in the horizontal and sagittal sections; iso-elevation contours are represented by thin lines in the transverse and sagittal sections. Abbreviations: a, anterior; c, contralateral; d, dorsal; i, ipsilateral; l, lateral; m, medial; p, posterior; v, ventral. From (Knudsen and Konishi, 1978) and (Konishi, 1986);

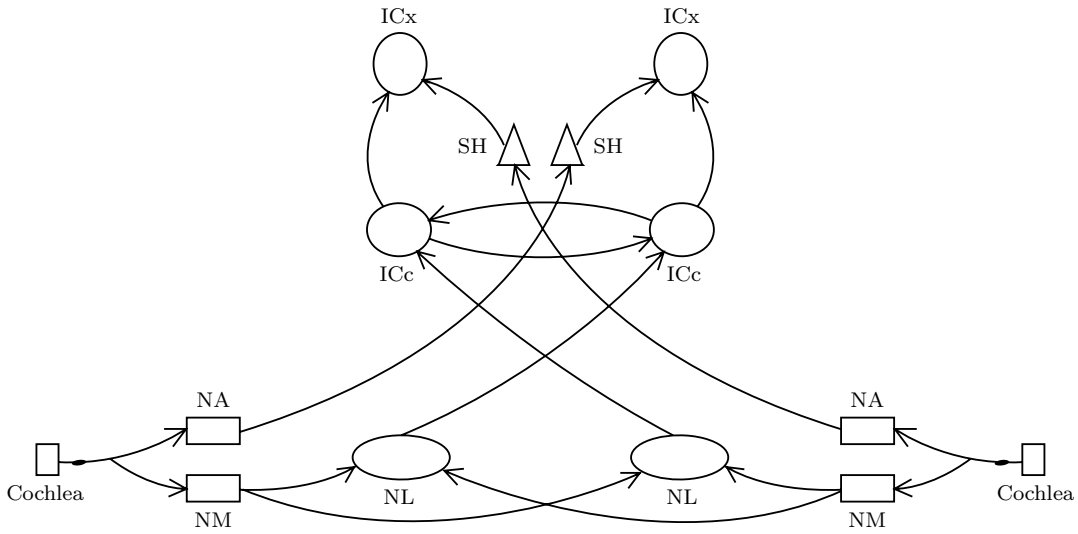

Figure 4.2. Schematic drawing of the auditory pathway of the barn owl. The pathway begins at the cochlea, the sound transducer. The cochlea projects to the nucleus angularis (NA), to start the amplitude-coding pathway, and to the nucleus magnocellularis (NM), to start the time-coding pathway. The NA projects contralaterally to the shell of central nucleus of the inferior colliculus (SH), which projects to the external nucleus of the inferior colliculus (ICx), the location of the complete map of auditory space. The NM projects bilaterally to nucleus laminaris (NL); the NL projects contralaterally to the central nucleus of the inferior colliculus (ICc). Fibers connect the ipsilateral and contralateral sides of the ICc, returning information to the original side. The ICc then projects to the ICx, the location of the complete map of auditory space. Adapted from (Fujita and Konishi, unpublished) and (Takahashi and Konishi, 1988b).

species and in mammals, although the most completely studied example of time-coding processing is that done by the barn owl.

The chapter describes a 220,000-transistor integrated circuit that models the time-coding pathway of the barn owl, using analog, continuous-time processing. The chip receives two inputs, corresponding to the sound pressure at each ear of the owl. The chip computes as its output a map of the interaural time difference between the input signals, encoding the azimuthal localization cue. The architecture of the chip directly reflects the anatomy and physiology of the neural pathway; intermediate outputs of the chip correspond to different neurons in this pathway. The original research in this chapter was done in collaboration with Carver Mead; parts of this chapter were originally published in (Lazzaro and Mead, 1989a).

4.1 The Time-Coding Pathway of the Owl

By installing small microphones near the eardrums of the owl, Moiseff and Konishi have demonstrated the dependence of binaural time difference on the azimuthal angle of a sound source (Figure 4.3). The time-coding pathway of the owl computes azimuth, using this binaural time difference as a cue.

The time-coding pathway receives as input a collateral of the primary auditory fibers. The primary auditory fibers originate at the cochlea; Chapter 2 described the structure and function of the cochlea. The mean firing rate of a primary auditory fiber encodes sound intensity. The temporal pattern of auditory-nerve firings reflects the shape of the filtered and rectified sound waveform; this phase locking does not diminish at high intensity levels (Evans, 1982). This temporal patterning preserves the timing information needed to encode interaural time differences.

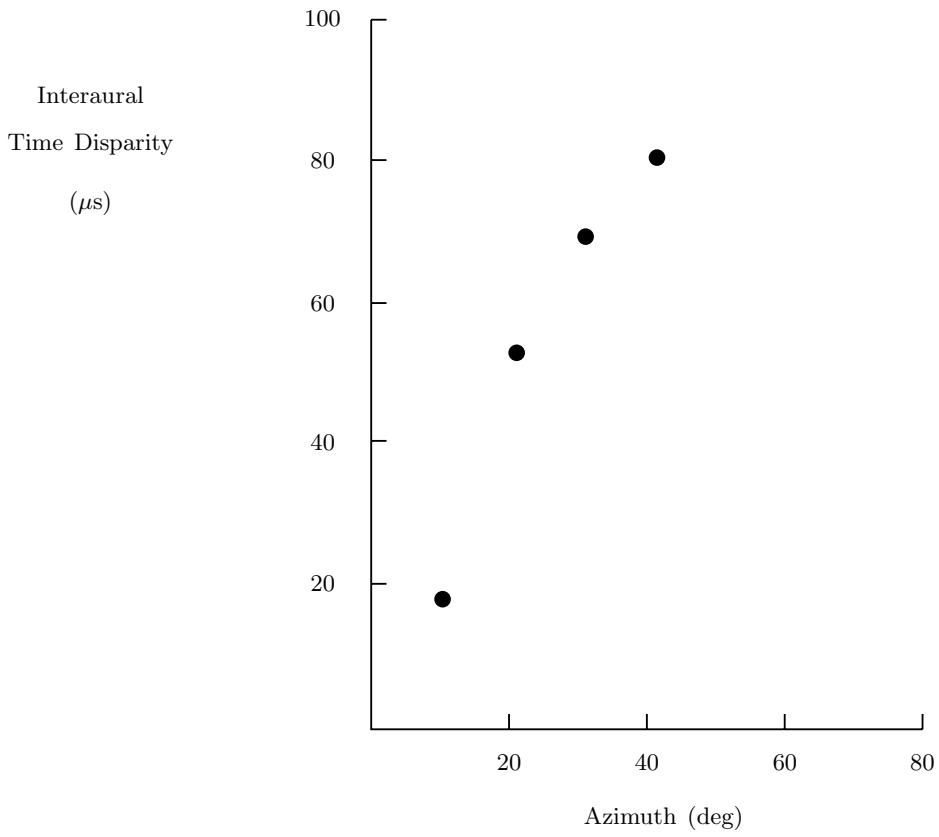

Figure 4.3. Binaural time difference in the owl, as a function of azimuthal angle. Small microphones installed near the eardrums were used to measure the interaural time differences in the microsecond range. From (Moiseff and Konishi, 1981).

In the owl, the primary auditory fibers project to the nucleus magnocellularis (NM), the first nucleus of the time-coding pathway (Figure 4.2). Neurons in the NM preserve the temporal patterning of nerve firings conveyed by the primary auditory fibers (Sullivan and Konishi, 1984). The NM projects bilaterally to the nucleus laminaris (NL), the first nucleus in the time-coding pathway that receives input from both ears. The mammalian homologue of the NL is the medial superior olive (MSO), which also receives input from both ears.

Neurons in both the NL (Moiseff and Konishi, 1983) and the MSO (Goldberg and Brown, 1969) are most sensitive to binaural sounds that have a specific interaural time delay (Figure 4.4). In 1948, Jeffress proposed a model to explain the encoding of interaural time differences in neural circuits (Jeffress, 1948). In the model, as applied to the anatomy of the owl, axons from the ipsilateral (same side) NM and the contralateral (opposite side) NM, with similar characteristic frequencies, enter the NL from opposite surfaces (Figure 4.5). The axons travel antiparallel, and action potentials counterpropagate across the NL; the axons act as neural delay lines. NL neurons are adjacent to both axons. Each NL neuron receives synaptic connections from both axons, and fires maximally when action potentials present in both axons reach that particular neuron at the same time. In this way, interaural time differences map into a neural place coding; the interaural time difference that maximally excites an NL neuron depends on the position of the neuron in the NL (Konishi, 1986). In engineering terms, each NL neuron computes the cross-correlation function of a filtered version of the sound inputs; the value of this function is the relative probability of the sounds being offset by a particular interaural time difference (Yin and Kuwada, 1984).

There is considerable evidence to support the application of this theory to the barn owl. Anatomical surveys of the NL of the owl show antiparallel axons, which enter from opposite sides, and which originate from the ipsilateral

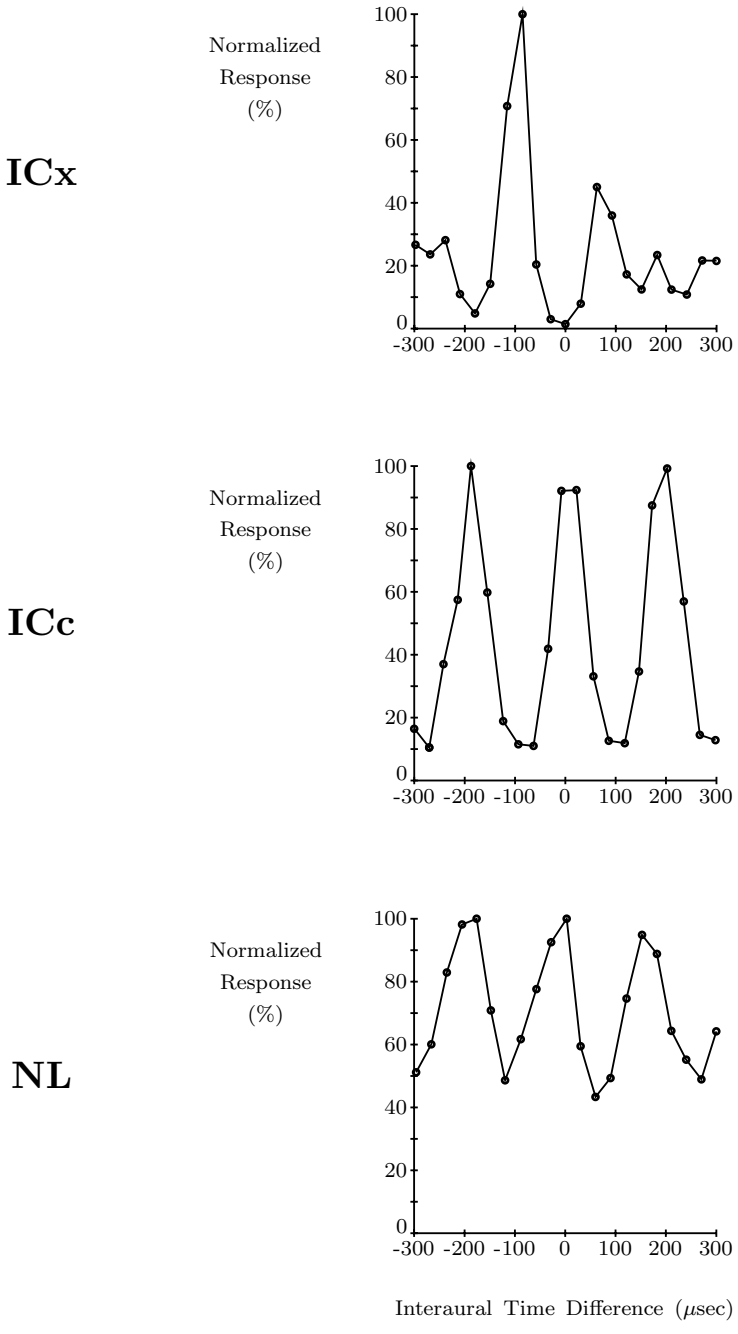

Figure 4.4. The delay curves obtained under physiological conditions from single units in the NL, the ICc, and the ICx. Broadband noise was used as a stimulus. Neurons with similar best frequencies (5.4 to 5.7 kHz) are shown. Neuronal selectivity improves markedly between the NL and the ICc. Responses are phase ambiguous in the NL and the ICc, but not in the ICx, when stimulated with noise. From (Fujita and Konishi, unpublished).

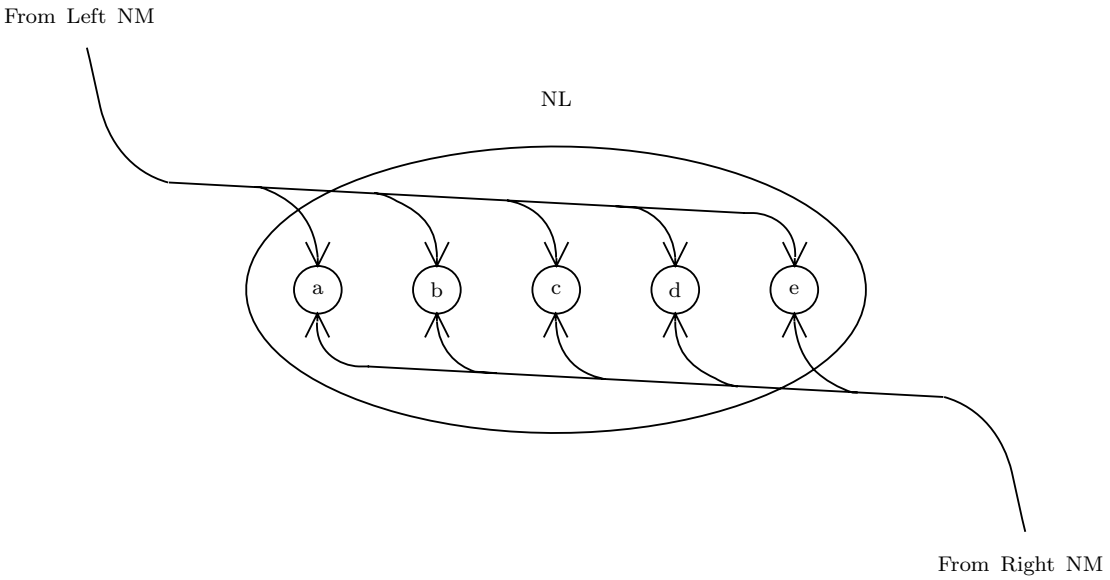

Figure 4.5. The Jeffress model for measuring and encoding interaural time differences, as applied to the barn owl. Fibers from the left and right NM converge on the NL; the NM fibers encode timing information in the temporal patterning of their action potentials. Each fiber has a uniform time delay. The NL neurons (circles labeled a through e) act as coincidence detectors, firing maximally when signals from two sources arrive simultaneously. The pattern of innervation of the NM fibers in the NL create left–right asymmetries in transmission delays; when the binaural disparities in acoustic signals exactly compensate for the asymmetry of a particular neuron, this neuron fires maximally. The position in the array thus encodes the interaural time difference. Adapted from (Konishi, 1986).

and contralateral NMs (Figure 4.6). Physiological data from NL neurons show a linear relationship between axonal time delay and axonal position in the NL (Carr and Konishi, 1988). Note that in Figure 4.4, NL neurons respond maximally to several different interaural time delays. As predicted by the Jeffress model, NL neurons respond to all interaural time differences that result in the same interaural phase difference of the characteristic frequency of the input fibers. In mammals, neuronal recordings in the MSO are also consistent with the Jeffress model (Goldberg and Brown, 1969).

NL outputs project contralaterally to a subdivision of the central nucleus of the inferior colliculus (ICc). ICc neurons are more selective for interaural time differences than are NL neurons (Figure 4.4); application of bicuculline methiodide (BMI, a selective gamma aminobtyric acid (GABA) antagonist) to the ICc reduces this improved selectivity. BMI acts as a blocker of inhibition; the action of BMI suggests that the increased selectivity of ICc neurons is a result of inhibitory circuits between neurons that are tuned to different interaural time differences (Fujita and Konishi, unpublished). Inhibitory circuits between neurons tuned to the same interaural time differences might also be present. In addition, evidence suggests that ICc neurons temporally integrate information to improve selectivity for interaural time differences. The sensitivity of ICc neurons to interaural time differences increases as a function of the duration of the sound stimulus, for sounds lasting less than 5 ms (Wagner and Konishi, unpublished).

The ICc projects to the external nucleus of the inferior colliculus (ICx), after crossing sides in the ICc. The ICx integrates information from the time-coding pathway and from the amplitude-coding pathway to produce a complete map of auditory space. Neurons in the ICx, unlike those in earlier stations of the time-coding pathway, respond to input sounds over a wide range of frequencies. ICx neurons are more selective for interaural time differences than are ICc neurons,

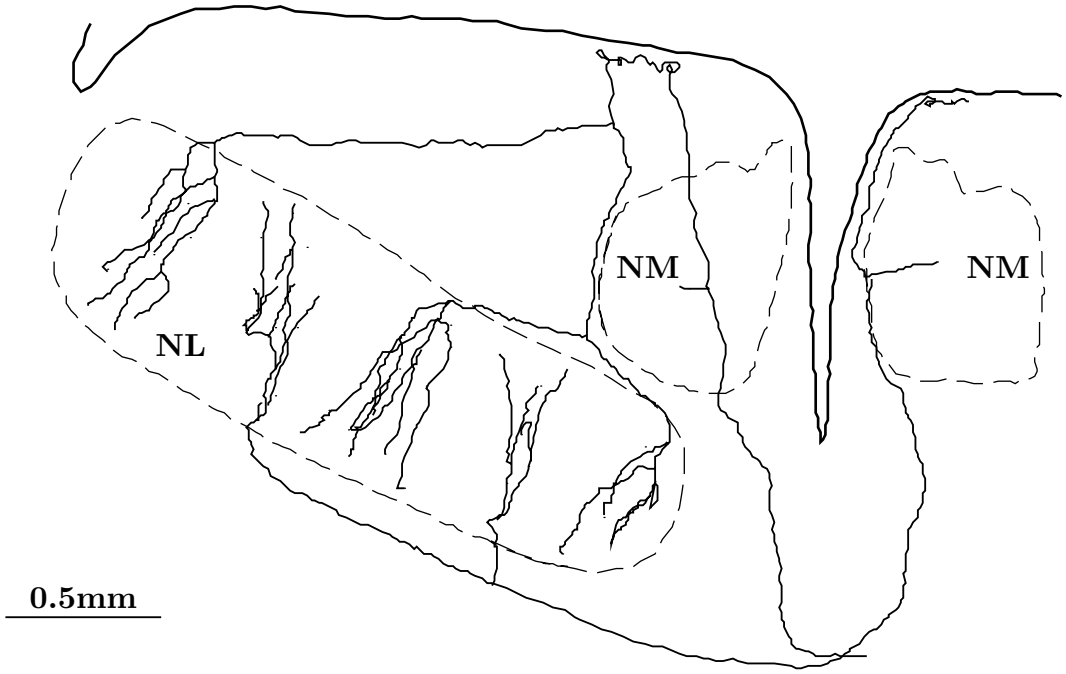

Figure 4.6. Innervation of nucleus laminaris. Axons from the ipsilateral and contralateral NM enter, respectively, the dorsal and ventral surfaces of the NL. Each axon runs along the respective surface until it comes to the iso-frequency band that it is destined to innervate. Within this band, the axon sends two or three collaterals into the NL, each of which divides into several branches. These fibers, which might be as long as 1 mm, run along a relatively straight course toward the opposite surface. The fibers appear to establish contacts with the NL cell bodies either by *en passant* endings or by small branchlets. From (Carr and Konishi, 1988) and (Konishi, 1986).

for low frequency sounds. In addition, neurons in earlier stations of the time-coding pathway respond to all interaural time differences that result in the same interaural phase difference of the neuron's characteristic frequency; neurons in the ICx respond maximally to one interaural time difference (Figure 4.4). This behavior suggests that ICx neurons combine information over many frequency channels in the ICc, to disambiguate interaural time differences from interaural phase differences. Application of BMI to the ICx results in phase ambiguity and decreased selectivity, suggesting an inhibitory mechanism for this computation (Fujita and Konishi, unpublished).

4.2 A Silicon Model of the Time-Coding Pathway

Figure 4.7 shows the floorplan of the silicon model of the time-coding pathway. The chip receives two inputs, corresponding to the sound pressure at each ear of the owl. Each input connects to a silicon model of the mechanical processing of the cochlea (Lyon and Mead, 1988a); Chapter 2 describes the cochlea model. Silicon models of inner hair cells connect to the cochlea circuit at constant intervals; 62 inner-hair-cell circuits connect to each silicon cochlea. The output of each inner-hair-cell model connects directly to a spiral-ganglion-neuron model, to complete a silicon model of auditory-nerve response. Chapter 2 described the auditory-nerve model. In the owl, the spiral-ganglion neurons project to the NM; for simplicity, our integrated circuit does not model the NM; each spiral-ganglion-neuron circuit directly connects to the NL.

In both owls and mammals, two instances of each nucleus in the auditory pathway appear in the brainstem, symmetric about the midline. Obviously, for binaural processing, two cochleas and two NMs are required. The NL, however, receives bilateral projection from the NM; each NL primarily encodes one-half of the azimuthal plane. This partitioning continues at higher stations;

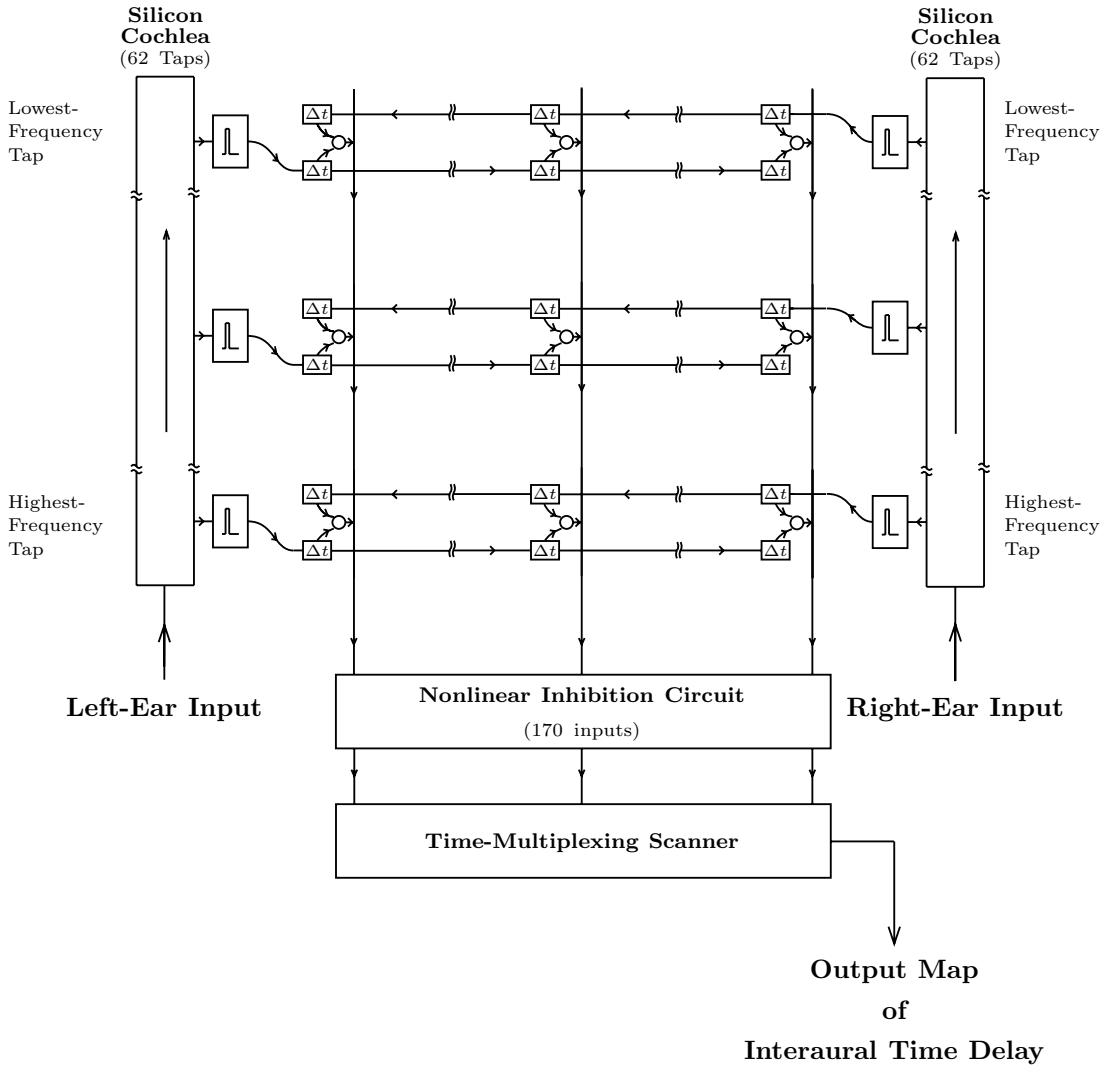
Silicon
Cochlea
(62 Taps)
Silicon
Cochlea
(62 Taps)
Lowest-
Frequency
Tap
Lowest-
Frequency
Tap
Highest-
Frequency
Tap
Highest-
Frequency
Tap
Δt
Left-Ear Input
Right-Ear Input
Nonlinear Inhibition Circuit
(170 inputs)
Time-Multiplexing Scanner
Output Map
of
Interaural Time Delay

Figure 4.7. Floorplan of the silicon model of the time-coding pathway of the owl. Sounds for the left ear and right ear enter the respective silicon cochleas at the lower left and lower right of the figure. Silicon inner hair cells tap each silicon cochlea at 62 equally spaced locations; each silicon inner hair cell connects directly to a silicon spiral-ganglion cell. The square box marked with a pulse represents both the silicon inner hair cell and the silicon spiral-ganglion cell. Each silicon spiral-ganglion cell generates action potentials; these signals travel down silicon axons, which propagate from left to right for silicon spiral-ganglion cells from the left cochlea, and from right to left for silicon spiral-ganglion cells from the right cochlea. The rows of small rectangular boxes, marked with the symbol "Δt," represent the silicon axons. One hundred seventy silicon NL cells, represented by small circles, lie between each pair of antiparallel silicon axons. Each silicon NL cell connects directly to both axons, and responds maximally when action potentials present in both axons reach that particular neuron at the same time. In this way, interaural time differences map into a neural place code. Each vertical wire that spans the array combines the outputs of all silicon NL neurons with a specific interaural time difference. These 170 vertical wires form a temporally smoothed map of interaural time difference, which responds to a wide range of input sound frequencies. The nonlinear inhibition circuit near the bottom of the figure increases the selectivity of this map. The time-multiplexing scanner transforms this map into a signal suitable for display on an oscilloscope.

for simplicity, our integrated circuit has only one copy of the NL and of later stations, which encodes all azimuthal angles.

The chip models the anatomy of the NL directly. The two silicon cochleas lie at opposite ends of the chip; the sounds in each silicon cochlea travel in parallel up the chip. Spiral-ganglion-neuron circuits from each ear, which receive input from inner-hair-cell circuits at the same cochlear position, project to separate axon circuits, which travel antiparallel across the chip. When a sound is presented to both chip inputs, action potentials counterpropagate across the chip.

The axon circuit is a discrete neural delay line; for each action potential at the axon's input, a fixed-width, fixed-height pulse travels through the axon, section by section, at a controllable velocity (Mead, 1989). After excitation of the circuit with a single action potential, only one section of the axon is firing at any point in time. NL neuron circuits lie between each pair of antiparallel axons at every discrete section, and connect directly to both axons. Simultaneous action potentials at both inputs excite the NL neuron circuit; if only one input is active, the neuron generates no output. This simplified model differs from the owl in several ways. The silicon NL neurons are perfect coincidence detectors; in the owl, NL neurons also respond, with reduced intensity, to monaural input. In addition, only two silicon axons converge on each silicon NL neuron; in the owl, many axons from each side converge on an NL neuron.

In the owl, the NL projects to the ICc, which in turn projects to the ICx. The final output of our integrated circuit models the responses of ICx neurons to interaural time differences. In response to interaural time differences, ICx neurons act different than NL neurons. Experiments suggest three mechanisms for these differences: nonlinear inhibition, temporal integration, and combining

of information over frequency channels. Our integrated circuit implements these mechanisms to produce a neural map of interaural time difference.

In our chip, all NL neuron outputs corresponding to a particular interaural time delay are summed to produce a single output value. NL neuron outputs are current pulses; a single wire acts as a dendritic tree to perform the summation. In this way, a two-dimensional matrix of NL neurons reduces to a single vector; this vector is a map of interaural time difference, for all frequencies. In the owl, inhibitory circuits between neurons tuned to the same interaural time differences might be present in the ICc, before combination across frequency channels. Our model does not include these circuits.

The ICc and perhaps the ICx might use temporal integration to increase selectivity. Our chip temporally integrates the vector that represents interaural time differences; the time constant of integration is adjustable. Nonlinear inhibitory connections between neurons tuned to different interaural time differences in the ICx and the ICc also increase sensitivity to interaural time differences. In our chip, a nonlinear inhibition circuit, described in Chapter 3, processes the temporally integrated vector that represents interaural time differences. The circuit performs a winner-take-all function, producing a new map of interaural time differences in which only one neuron has significant energy. The chip time multiplexes this final map of interaural time differences on a single wire for display on an oscilloscope.

4.3 Comparison of Responses

We presented periodic click stimuli to the chip; one input received the sound directly, while the other input received a time-delayed replica of the sound (Figure 4.8). We recorded chip response at several intermediate outputs and at the final output map of interaural time differences, and compared chip response

to similar responses recorded from the time-coding pathway of the barn owl. We also separately fabricated and tested several parts of the complete model.

Figure 4.9 shows the basilar-membrane response of the chip to click stimuli, with no interaural time difference. The figure shows output response at several equally spaced basilar-membrane locations, for both left and right cochleas. The frequency content of the response progressively decreases at locations farther from the beginning of the cochlea; in addition, the response at each location has a slight resonant overshoot. The response also shows a time delay between each pair of adjacent locations; for more distant locations, this time delay exceeds the period of the input waveform. These observations match the behavior of the traveling wave structure of physiological cochleas; a comparison of the responses of the physiological and silicon cochleas was given in Chapter 2.

The left and right cochlea responses are nearly identical; there are small differences in the velocity of propagation, due to imperfections in the circuit elements. Because of these differences, the time delays in the left and right cochleas at a particular location are not equal; these differences, shown in Figure 4.9, are a potential source of localization error.

Chapter 2 compared the responses of the silicon auditory-nerve model with physiological data. As shown in Figures 2.3, 2.8, and 2.10, a silicon auditory-nerve fiber encodes a filtered, half-wave-rectified version of the cochlea input, over a wide dynamic range, using the temporal patterning of fixed-width, fixed-height pulses. This property is vital for the correct function of the silicon model of the time-coding pathway. Figure 2.8(b) shows that the absolute phase of the temporal firing patterns of a silicon auditory nerve fiber shifts with input intensity, for high signal levels; this behavior is unlike a physiological fiber. Because of this shortcoming, we did not apply binaural intensity differences to the chip.

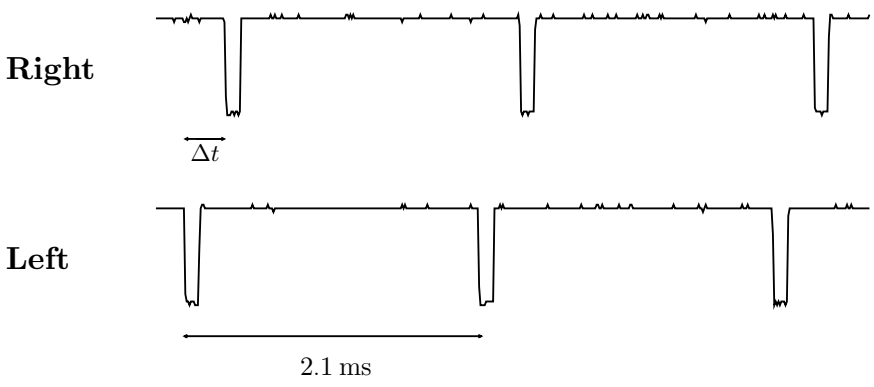

Figure 4.8. Input stimulus for the chip. Both left and right ears receive a periodic click waveform, at a frequency of 475 Hz. The time delay between the two signals, denoted by "Δt," is variable.

Input

L

R

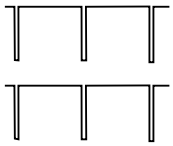

Tap 1

L

R

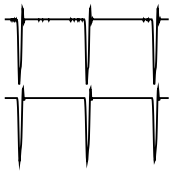

$\Delta t_o = -10\,\mu\text{s}$

Tap 2

L

R

$\Delta t_o = -46\,\mu\text{s}$

Tap 3

L

R

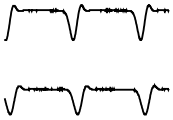

$\Delta t_o = -143\,\mu\text{s}$

Tap 4

L

R

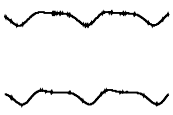

$\Delta t_o = -102\,\mu\text{s}$

Tap 5

L

R

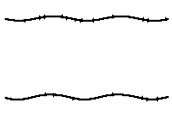

$\Delta t_o = +82\,\mu\text{s}$

Figure 4.9. Response of both cochleas to the input stimulus of Figure 3.8; this stimulus is reproduced at the top of this figure. The horizontal axis is time; each vertical axis is cochlear response. The figure shows the output response at five cochlear positions, for both left and right cochleas. Tap 1 is closest to the beginning of the cochlea, and retains most of the high-frequency content of the signal. Later taps show less and less high-frequency content; tap 5 contains only the fundamental frequency of 475 Hz. Each tap accentuates a particular frequency, the characteristic frequency of the cochlear position; this frequency decreases with increasing tap numbers. The cochleas act also as exponentially tapered delay lines; notice the response of each tap occurs progressively further from the input waveform. For taps 4 and 5, the delay of the cochlea exceeds a single period of the input waveform. The cochleas are not exactly matched; a difference in time delay between the two cochleas is denoted by "Δt_o," on the right of each pair of outputs. For lower-numbered taps, the delay is small compared to the time delay of the silicon axons; for higher-numbered taps, it is significant.

Figure 4.10 shows the output of several sections of the axon circuit, in response to a single input pulse. Only one section is active at any point in time; the pulse width does not grow or shrink systematically, but rather stays roughly constant. Figure 4.11 shows the variation in axon pulse width over about 100 sections of axon, due to circuit element imperfections. In this circuit, a variation in axon pulse width indicates a variation in the velocity of axonal propagation; this variation is a potential source of localization error.

The final output of the chip is a map of interaural time difference. Three signal-processing operations, computed in the ICx and ICc, improve the original encoding of interaural time differences in the NL: temporal integration, integration of information over many frequency channels, and inhibition among neurons tuned to different interaural time delays. In our chip, we can disable the inhibition and temporal-integration operations, and observe the unprocessed map of interaural time differences.

Figure 4.12(a) shows these unprocessed maps of interaural time differences, created in response to click stimuli. Each map corresponds to an interaural time difference that is 100 μs greater than that for the previous map; the first map corresponds to simultaneous excitation of both ears. The vertical axis of each map corresponds to neural activity level, whereas the horizontal axis of each map corresponds to linear position within the map. Each map is an average of several maps recorded at 100-ms intervals; averaging is necessary to capture a representation of the quickly changing, temporally unsmoothed response. The encoding of interaural time differences is present in the maps, but false correlations add unwanted noise to the desired signal. By combining the outputs of 62 rows of NL neurons, each tuned to a separate frequency region, the maps in Figure 4.12(a) correctly encode interaural time differences, despite variation in axonal velocity, mismatches in cochlear delay, and noise.

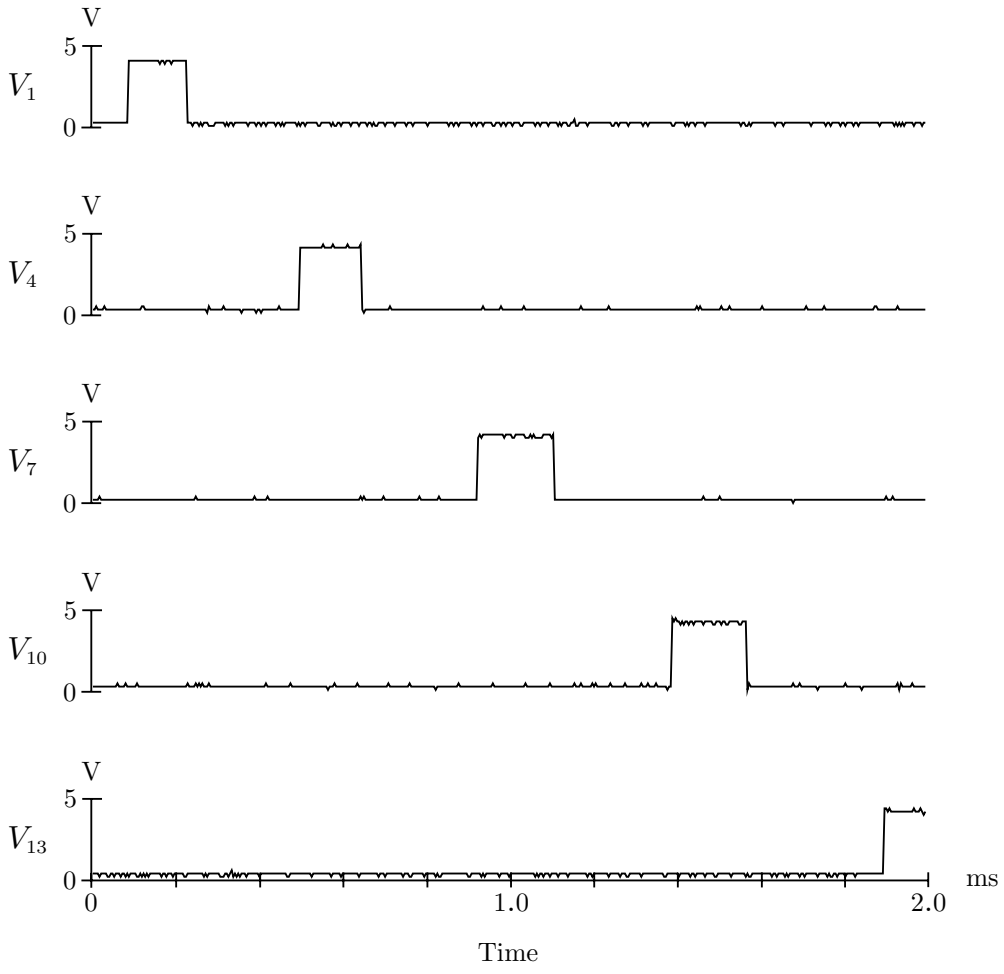

Figure 4.10. Waveform measured at several sections of a silicon axon. Outputs were located at every third section; thus, two outputs are not shown for every one that is. Note that pulse height and pulse width stay fairly constant, and that only one axon section is active at any point in time. From (Mead, 1989).

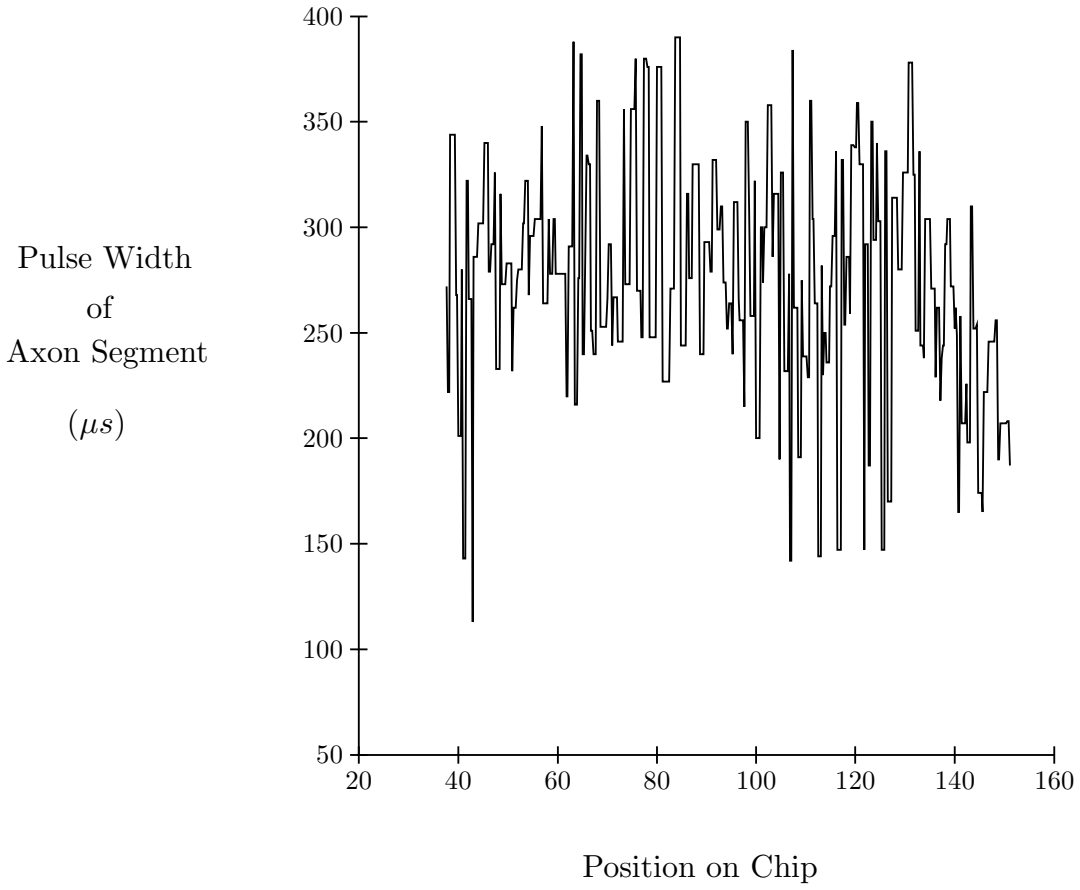

Figure 4.11. Variation in the pulse width of a silicon axon, over about 100 axonal sections. Axons were set to fire at a slower velocity than in the owl model, for more accurate measurement. The line represents the section-by-section pulse width.

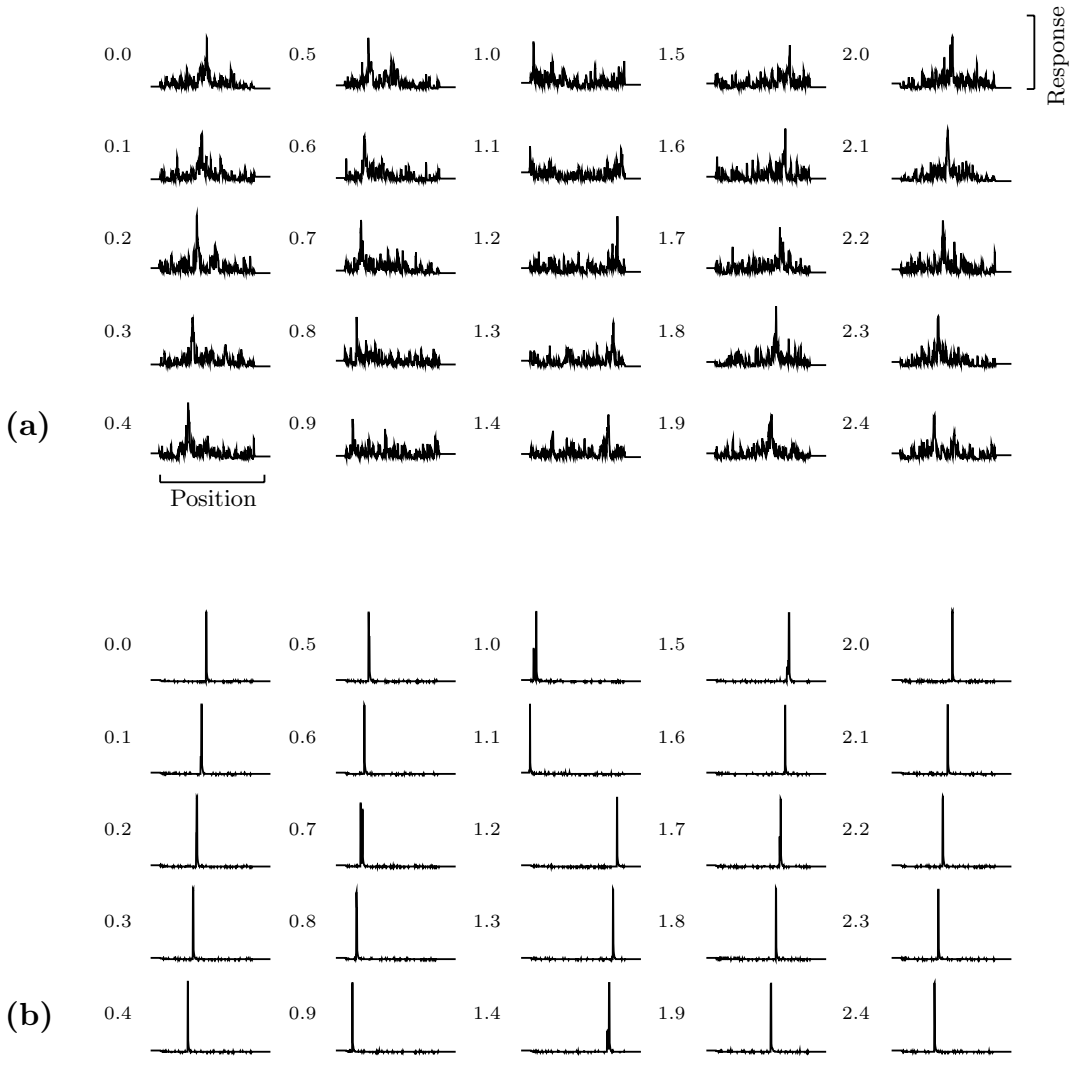
0.0
0.5
1.0
1.5
2.0
0.1
0.6
1.1
1.6
2.1
0.2
0.7
1.2
1.7
2.2
0.3
0.8
1.3
1.8
2.3
0.4
0.9
1.4
1.9
2.4
Position
Response
(a)
(b)

Figure 4.12. Maps of interaural time differences, taken from the chip. **a.** The nonlinear inhibition and temporal smoothing operations were turned off, showing the unprocessed map of interaural time delays. Each individual plot shows the neural response at every position across the map. The stimuli for each plot are the periodic click waveforms, offset by an interaural time difference, shown in Figure 4.8; the interaural time difference is shown in the upper-left corner of each plot, measured in milliseconds. These responses are the averaged result of four maps, at 100-ms intervals, using a digital oscilloscope, because the on-chip temporal smoothing is disabled. The encoding of interaural time differences is present in the maps, but false correlations add unwanted noise to the desired signal. Because we are using a periodic stimulus, large time delays are interpreted as negative delays, and the map response wraps from one side to the other at an interaural time difference of 1.2 ms. **b.** The nonlinear inhibition and temporal-smoothing operations were turned on, showing the final output map of interaural time delays. Format is identical to that in part a. Off-chip averaging was not used, because the chip temporally smooths the data. Each map shows a single peak, with little activity at other positions, due to nonlinear inhibition.

Figure 4.12(b) shows maps of interaural time differences taken with inhibition and temporal-integration operations enabled, using stimuli identical to those for Figure 4.12(a). For most interaural time differences, only one peak exists. Off-chip averaging of maps over time is not necessary, as the temporal-integration operation on the chip smooths the time response of the chip. The maps do not reflect the periodicity of the individual frequency components of the sound stimulus; experiments with a noise stimulus confirm the phase-disambiguation property of the chip.

Figure 4.13(a) is an alternative representation of the map of interaural time differences computed by the chip. We recorded the map position of the neuron with maximum signal energy, for different interaural time differences, using periodic click stimuli. Carr and Konishi (Carr and Konishi, 1988) performed a similar experiment in the NL of the barn owl (Figure 4.13b), mapping the time delay of an axon innervating the NL, as a function of position in the NL. The linear properties of our chip map are the same as those of the owl map.

4.4 Discussion

The experiments on the chip raise several interesting issues about the algorithms implemented by the auditory-localization system of the barn owl. These issues concern the computational errors that occur due to imperfect components, and how nature might attempt to correct for these errors.

Figure 4.9 shows the responses of two silicon cochleas to a click stimulus. Because of component imperfections, the delays at the same position on the two silicon cochleas are not identical. As a result, the row of NL neuron circuits associated with this position has a spatial offset; in response to an interaural time difference of zero, the NL neuron circuit with maximum energy is not located exactly in the center of the row. If each cochlear position has a different

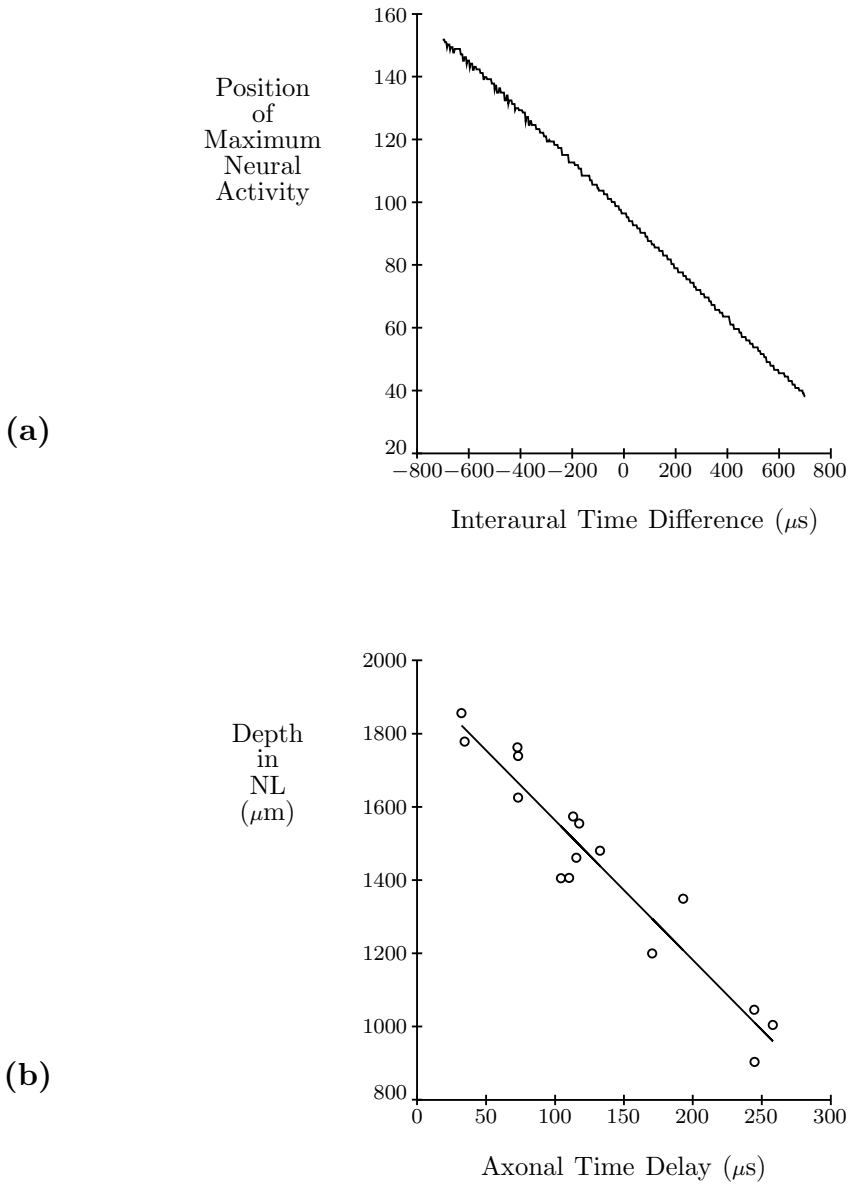

Figure 4.13. a. Chip data showing the linear relationship of silicon NL neuron position and interaural time difference. For each interaural time difference presented to the chip, the output map position with the maximal response is plotted (170 map positions). The linearity shows that silicon axons have a uniform mean time delay per section. **b.** Recordings of the NM axons innervating the NL in the barn owl. The figure shows the mean time delays of contralateral fibers recorded at different depths during one penetration through the 7-kHz region. From (Carr and Konishi, 1988).

temporal offset, each row of NL neurons has a different spatial offset; thus, the two-dimensional silicon NL map is not correctly registered in the place dimension.

This incorrect registration is a problem because the projection to the silicon model of ICx and ICc is hardwired; there is no mechanism to adapt to the offsets in the silicon NL map. The biological system might also have the same interaural matching problem; to solve the problem, the system might use adaptation. Adapting time delays in the system could result in a well-registered NL map; in addition, adaptive projections from the NL to higher centers could decrease registration errors in the NL map.

Figure 4.11 shows the variation in propagation velocity of a silicon axon. This variance is a potential source of localization error. The error in the output map of the chip from this error is minimized as a byproduct of the processing algorithm of the system; the output map averages the responses of 62 rows of NL neurons. In the biological system, ICx neurons combine information over many frequency channels in the ICc; this operation also reduces errors in individual ICc responses. In addition, the axons innervating NL might adapt to reduce the variance in their propagation velocity, eliminating the source of the error.

Future enhancements of the chip include modeling these methods of adaptation to improve system performance, modeling the intensity-coding localization pathway, and using the chip as part of a electromechanical system to model sensorimotor integration in the owl. In conclusion, the chip confirms the plausibility of the model of time-coding pathway of the owl formulated by Konishi and collaborators. The chip also demonstrates the utility of analog VLSI technology as a modeling tool in computational neuroscience.